Supplement of Biogeosciences, 21, 3271–3288, 2024
https://doi.org/10.5194/bg-21-3271-2024-supplement

Biogeosciences Open Access EGU

Supplement of

Composite calcite and opal test in Foraminifera (Rhizaria)

Julien Richirt et al.

Correspondence to: Julien Richirt (richirt.julien@gmail.com)

Method S1

Conventional quantitative EDS analyses uses ZAF method for correction by atomic number (Z), absorption (A) and X-ray fluorescence (F), assuming that the surface is completely flat and elemental composition along with depth direction is homogeneous. However, our cryo-SEM-EDS maps does not meet these requirements, and the apparent EDS maps are correlated with background, as indicated by the similarity between count-per-second (CPS) maps and the EDS maps of low-intensity elements. Several factors cause the inhomogeneous CPS, such as position-dependent electron penetration depth and electron scatter within the specimen. Therefore, the aim of this correction procedure is to minimise the position-dependent background signal.

EDS maps are generated from the number of counts where X-rays from atom A appears, and the counts I_A is composed of pure signal S_A and background B_A, mostly composed of bremsstrahlung effect. Because of B_A, EDS maps show random noise-like background, whose intensity is correlated with the CPS. CPS represent the sum of signals of all the atoms and the background:

$$\mathrm{CPS} = \Sigma_i S_i + B = \Sigma_i I_i + B_{\bar{\imath}}$$

With *i* the atom of interest, *B* the summation of the background intensity at all the energy, and $B_{\bar{\imath}}$ the summation of the background intensity at energy ranges where characteristic X-ray peaks are absent. The background mostly comes from bremsstrahlung effect, thus is dependent on beam condition. Here, we assume that the background shape is the same in any position of EDS maps. The intensity-to-noise ratio *R* of an atom *i* at position (*m*, *n*) is then defined as:

$$R(m,n) = \frac{I_i(m,n)}{B_i(m,n)} = \frac{S_i(m,n)}{B_i(m,n)} + 1 = \frac{I_i(m,n)}{\mathrm{CPS} - \Sigma_i I_i(m,n)}$$

which is related to the conventional signal-to-noise ratio S_i/B_i. We used *R* to map elements.

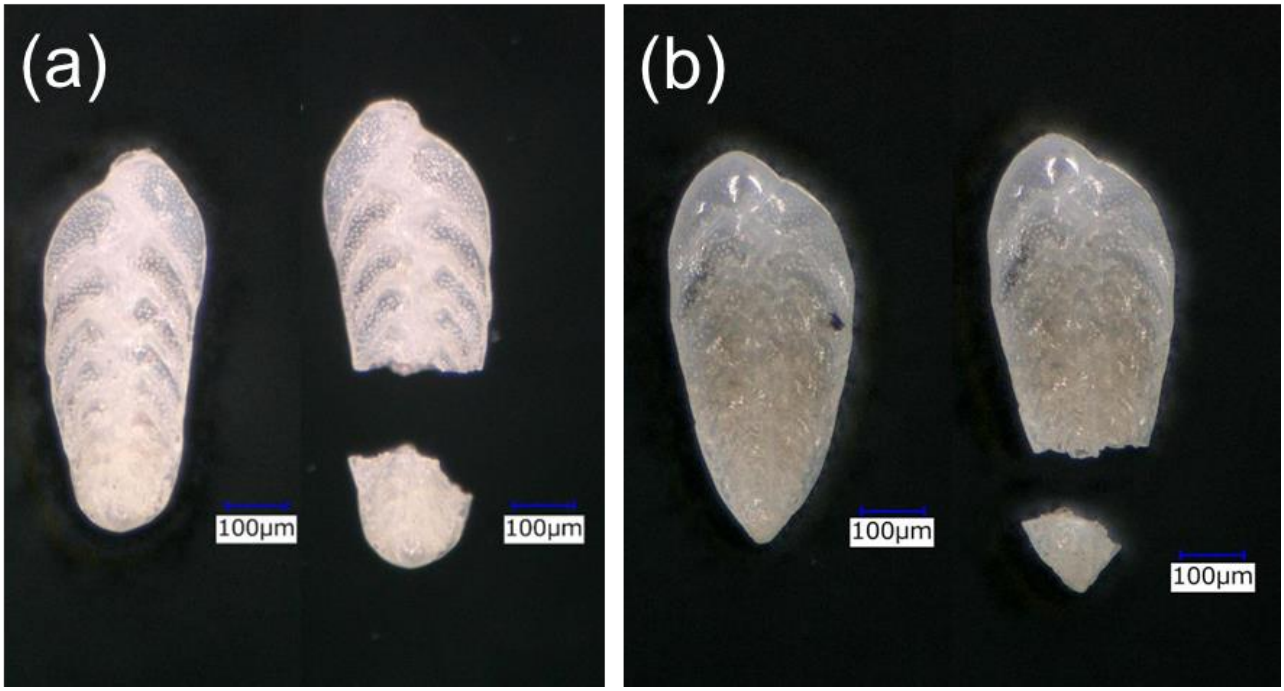

Fig. S1: Stereomicroscope image of the macrospheric (a) and microspheric (b) *Bolivina spissa* from NSB station before and after dissection prior isotopic composition measurement.

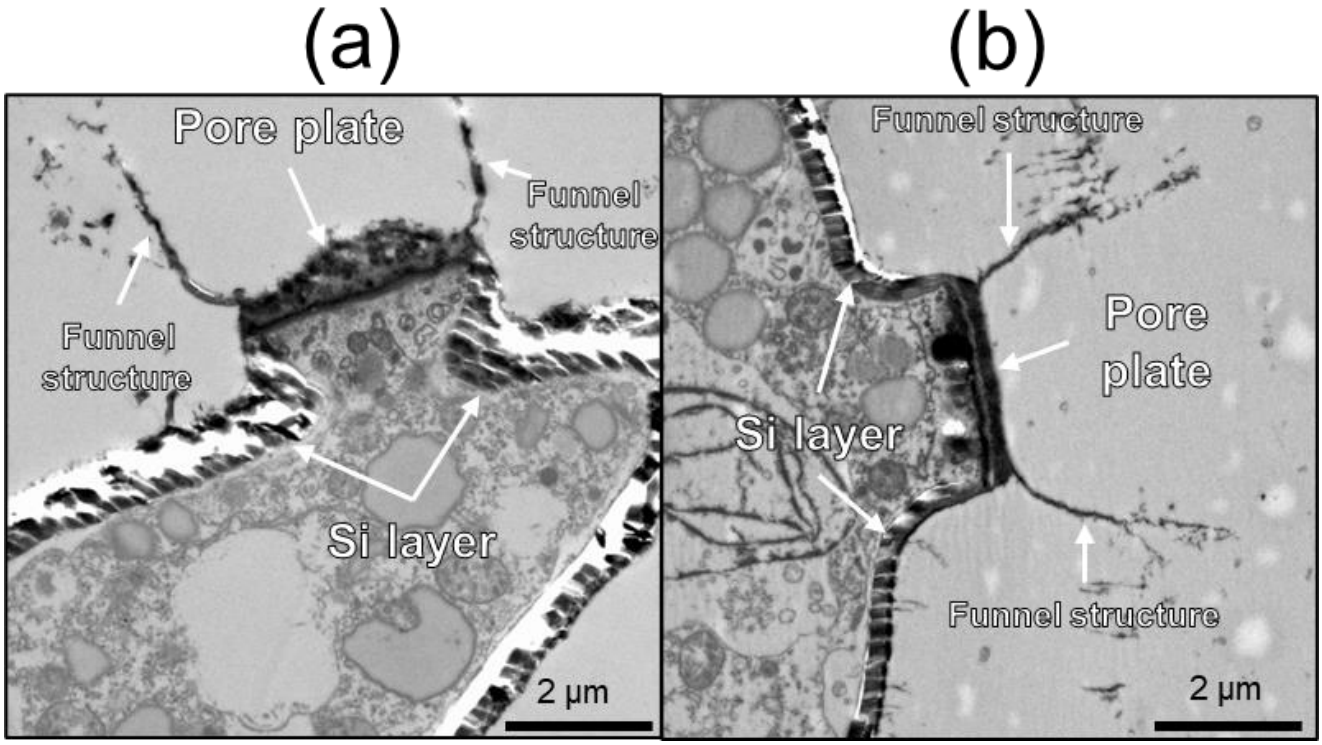

Fig. S2: (a and b) two ultrathin sections of *B. spissa* imaged with TEM showing pore area, with the pore plate and the Si layer. The "funnel" structures, coating the inner surface of the original pore's calcitic wall before decalcification, are also visible.

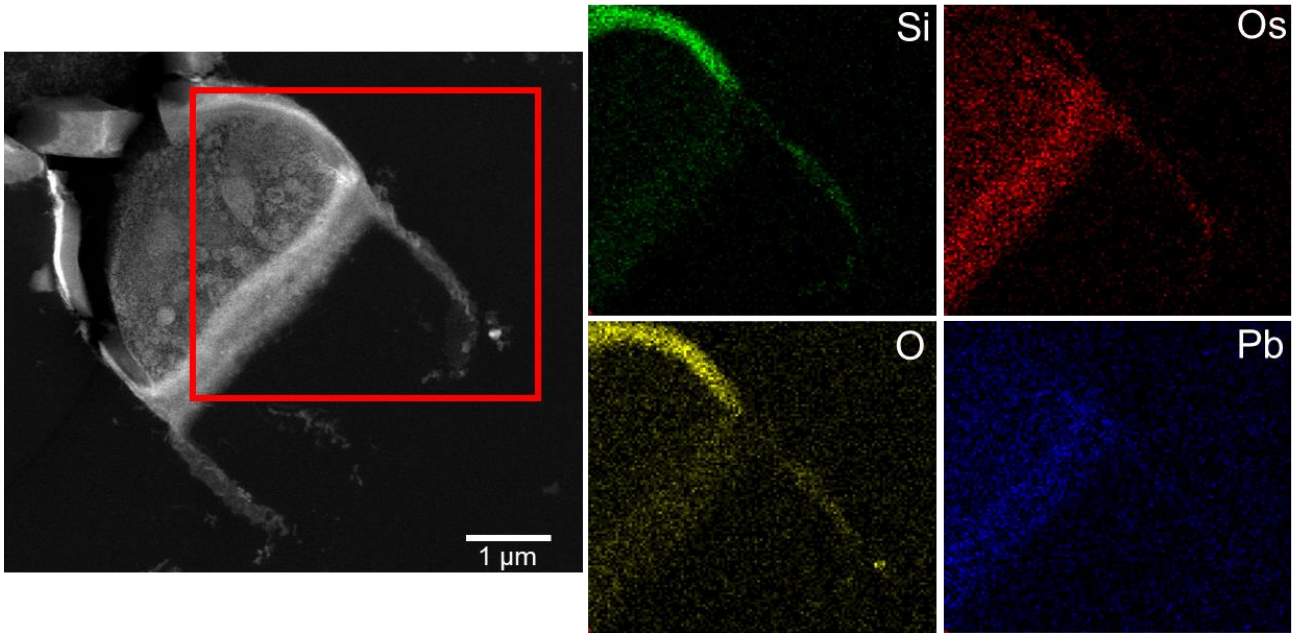

Fig. S3: STEM-EDS image from a pore region of *B. spissa* after decalcification. EDS maps of the region framed by the red rectangle for elements Si, O, Os and Pb. Si and O are the main component of the Si layer coating the inside part of the pore. Os and Pb distribution are indicating organic matter, such as the pore plate. Note that funnel-structures and the pore plate are not Si enriched.

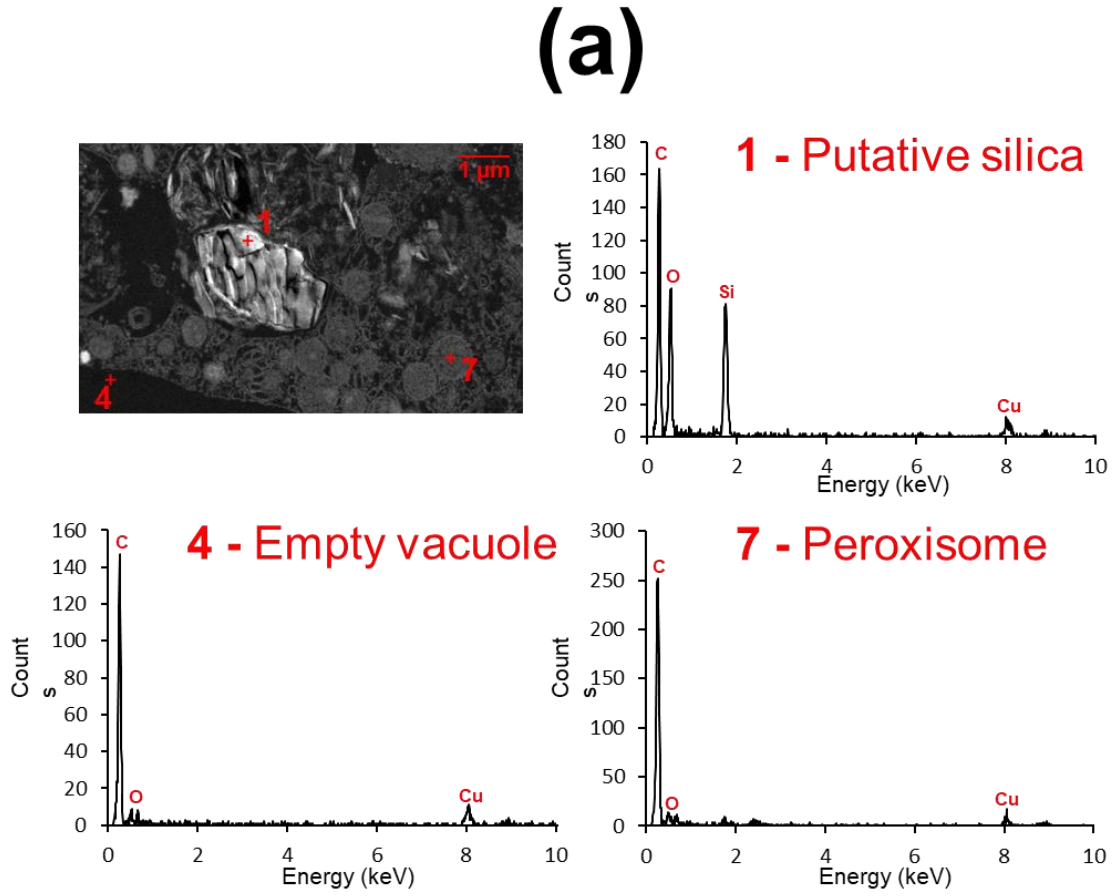

Fig. S4: point measurement EDS performed on ultrathin sections of *B. spissa* imaged with STEM. (a) spectra from putative SDV content (1), an empty vacuole (4) and a peroxisome (7). (b) spectra from putative SDV content (1 and 4) and the Si layer coating the inside part of the calcitic shell (5). (c) Spectra from the content in sediment vesicle filled with sediment particles (2 and 3) and organic matter (6). Cu signal is from the TEM support grid.

(b)

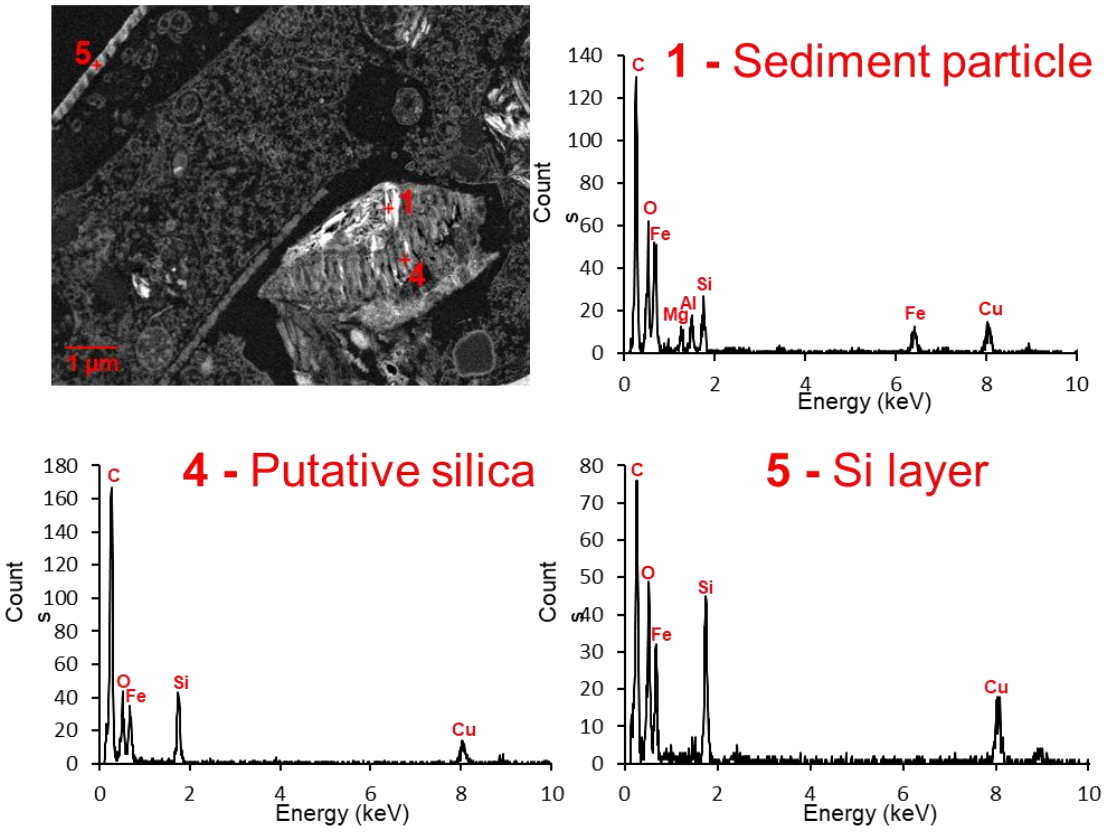

Fig. S4: continued

(c)

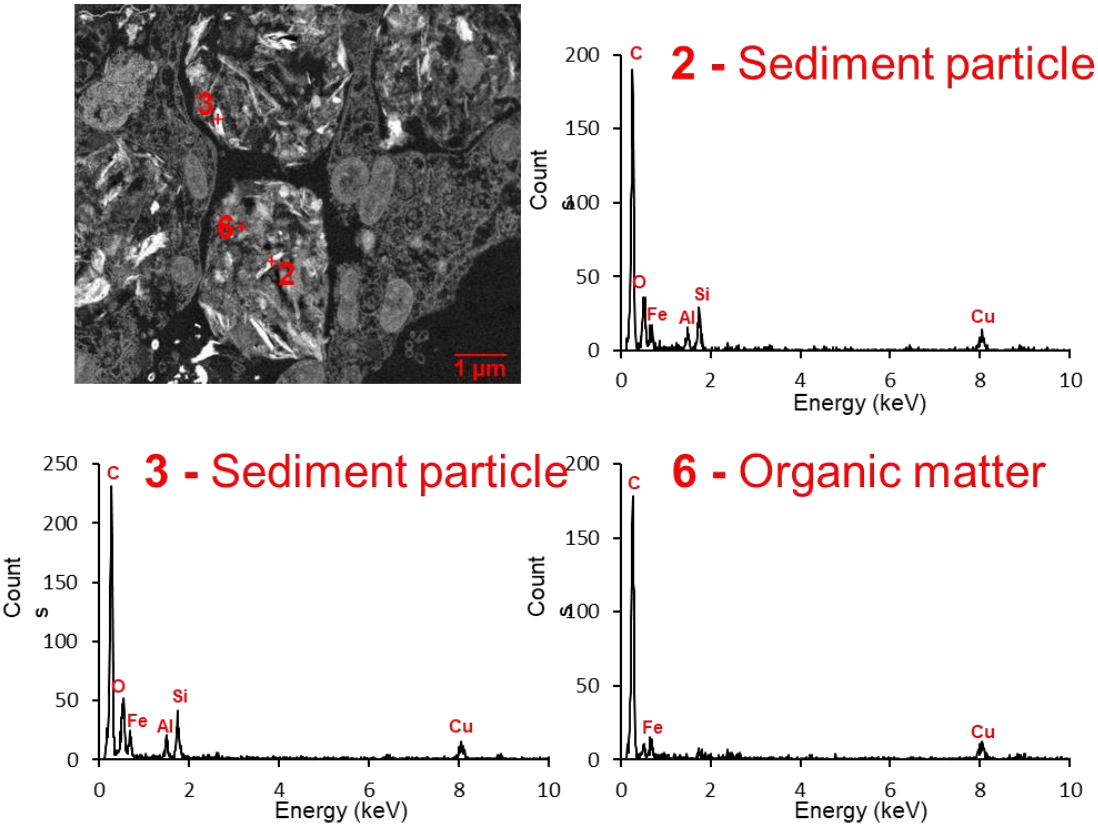

70

Fig. S4: continued

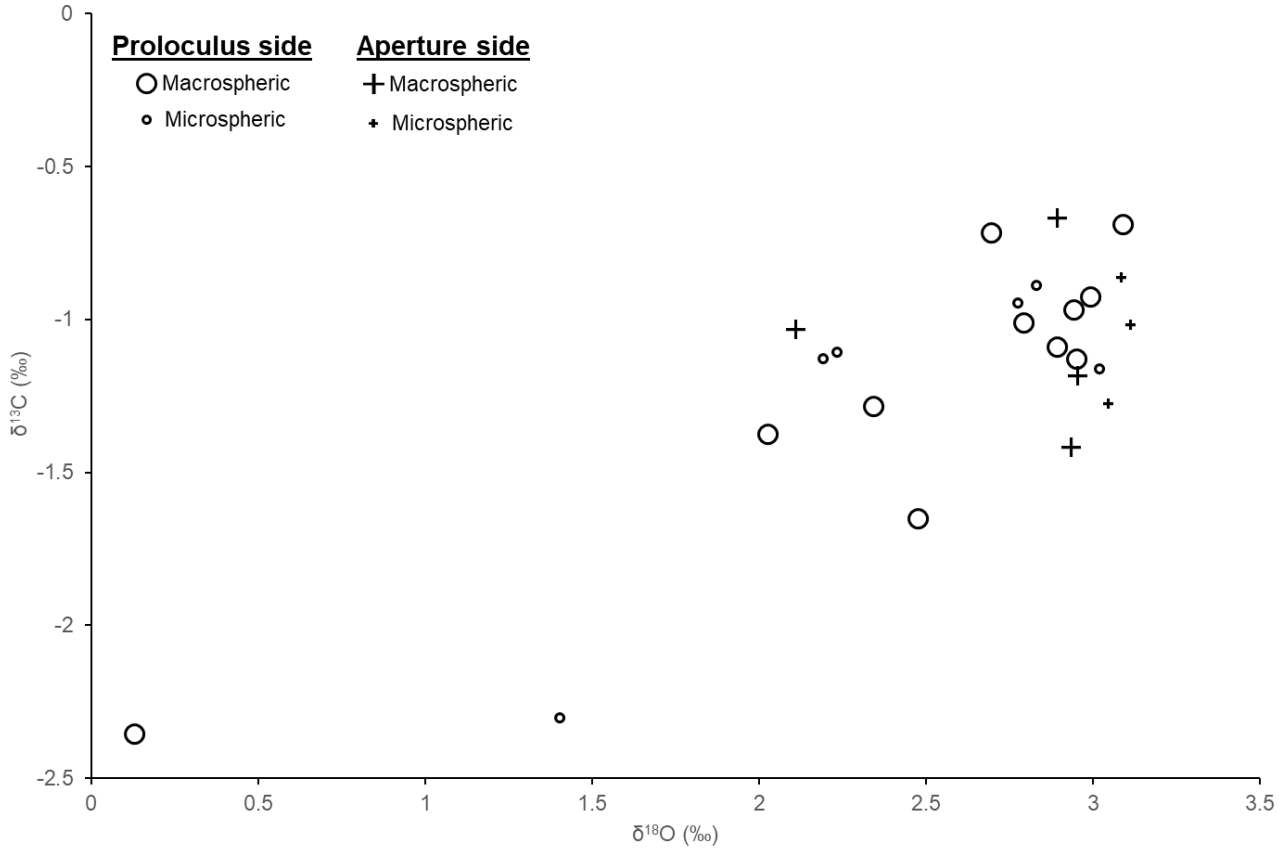

Fig. S5: Stable carbon ($\delta^{13}C$) and oxygen ($\delta^{18}O$) isotopic compositions of calcite measured after microdissection of individuals to separate the oldest chambers on the proloculus side (circles) and on the aperture side (crosses). The size of symbols indicates if the individuals was macrospheric (large symbol) or microspheric (small symbol).

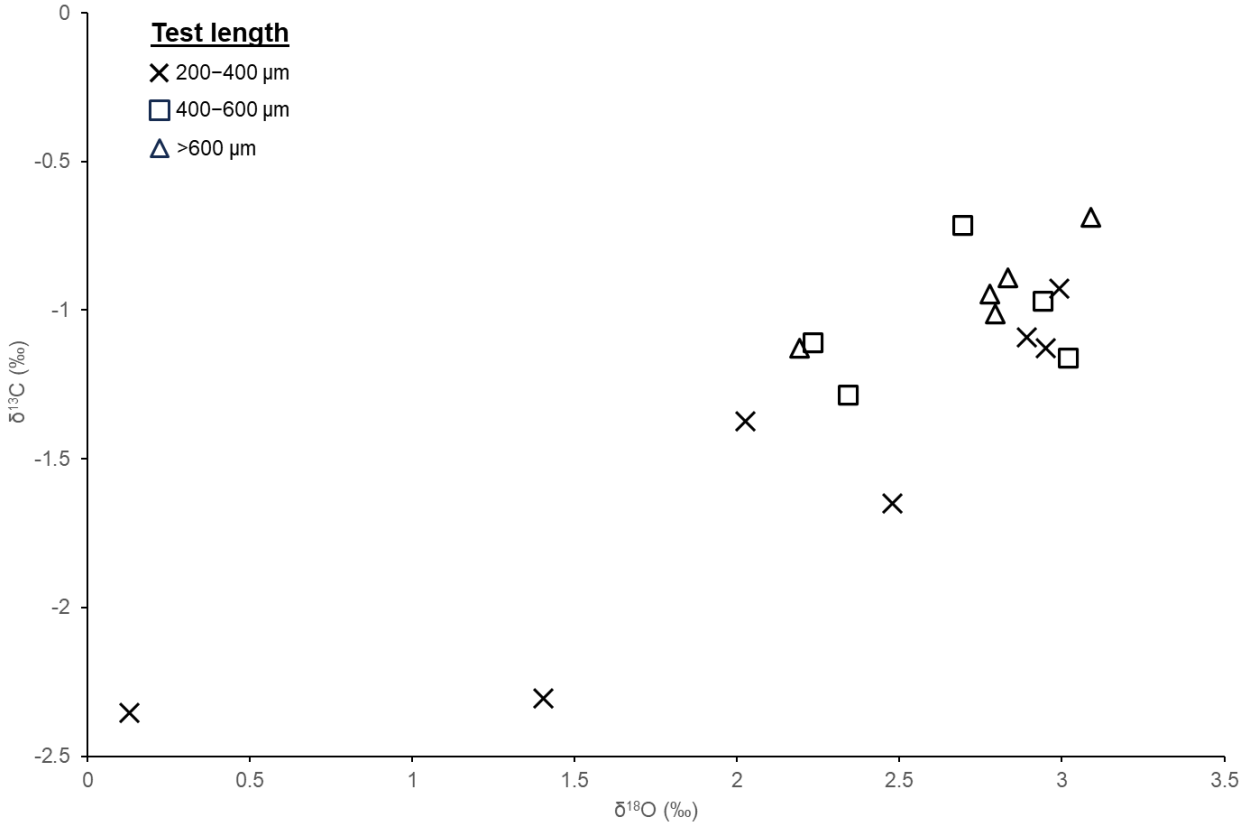

Fig. S6: Stable carbon ($\delta^{13}C$) and oxygen ($\delta^{18}O$) isotopic compositions of calcite measured on the proloculus side and total length of individual tests measured. Crosses=200-400 µm, squares=400-600 µm) and triangles= >600 µm.

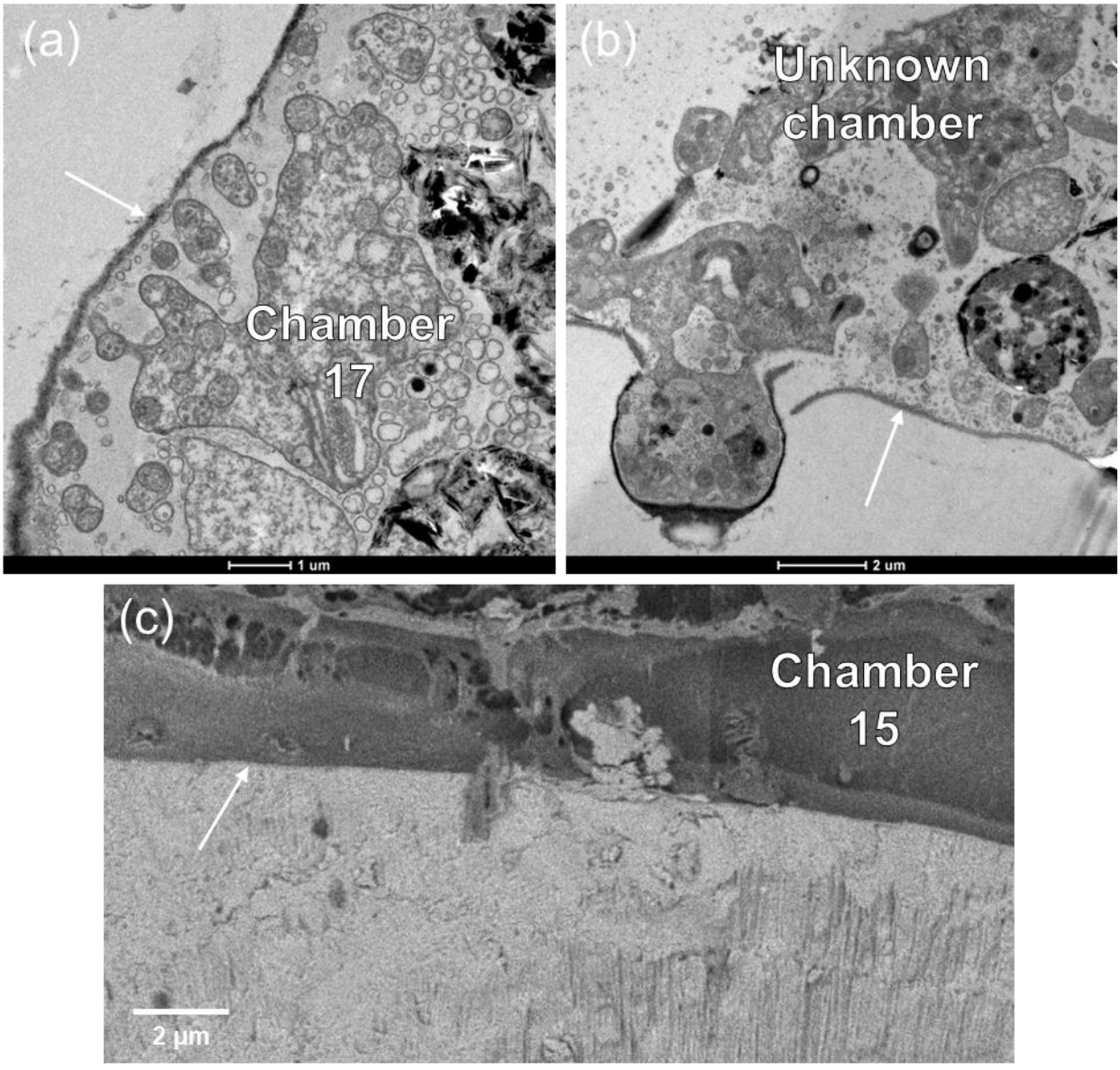

Fig. S7: TEM images of the chamber edges of (a) chamber 17 and (b) a chamber of unknown number (because the proloculus was not visible) in two different individuals, and (c) cryo-SEM image of the chamber edge of chamber 15 of *B. spissa* specimen from NSB station, all showing the absence of Si layer. White arrows indicate the regions of interest.

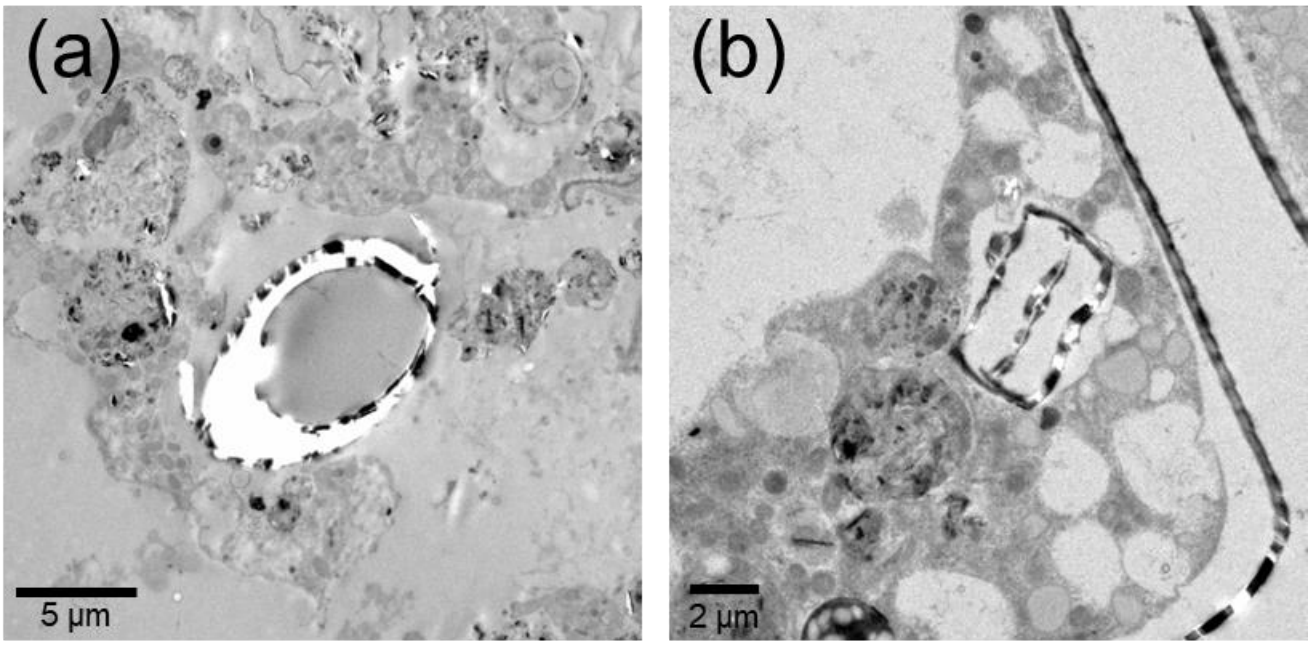

Fig. S8: (a and b) Examples of TEM images of the cellular content of *Bolivina spissa* from NSB station showing empty diatom frustule remains.

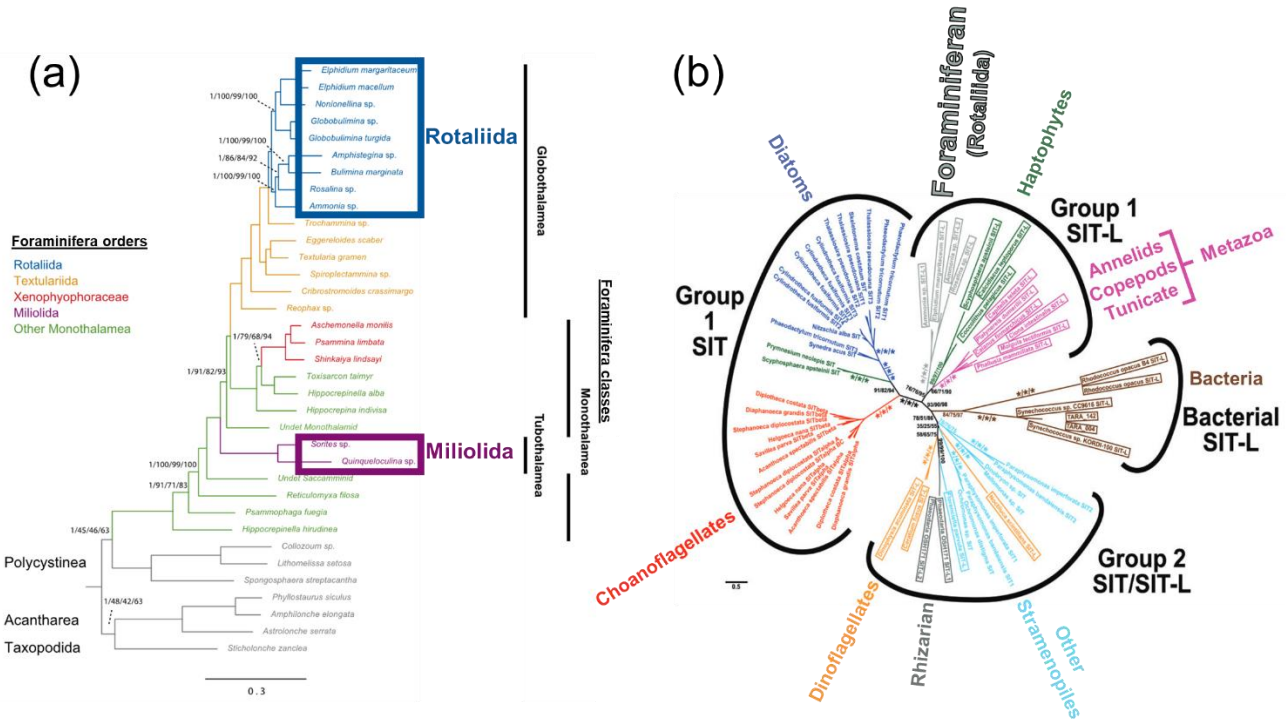

110 **Fig. S9: (a) Phylogenetic tree corresponding to the best ML tree and Bayesian inference from a concatenated analysis of 199 proteins showing all major groups of Foraminifera with Rotaliida in blue and Miliolida in purple (modified from Sierra et al., 2022). (b) Phylogenetic tree based on Si transporter sequences (modified from Marron et al., 2016). Foraminifera (grey), all belonging to the order Rotaliida such as *Bolivina*, are branching with Haptophyta and different Metazoa.**

115

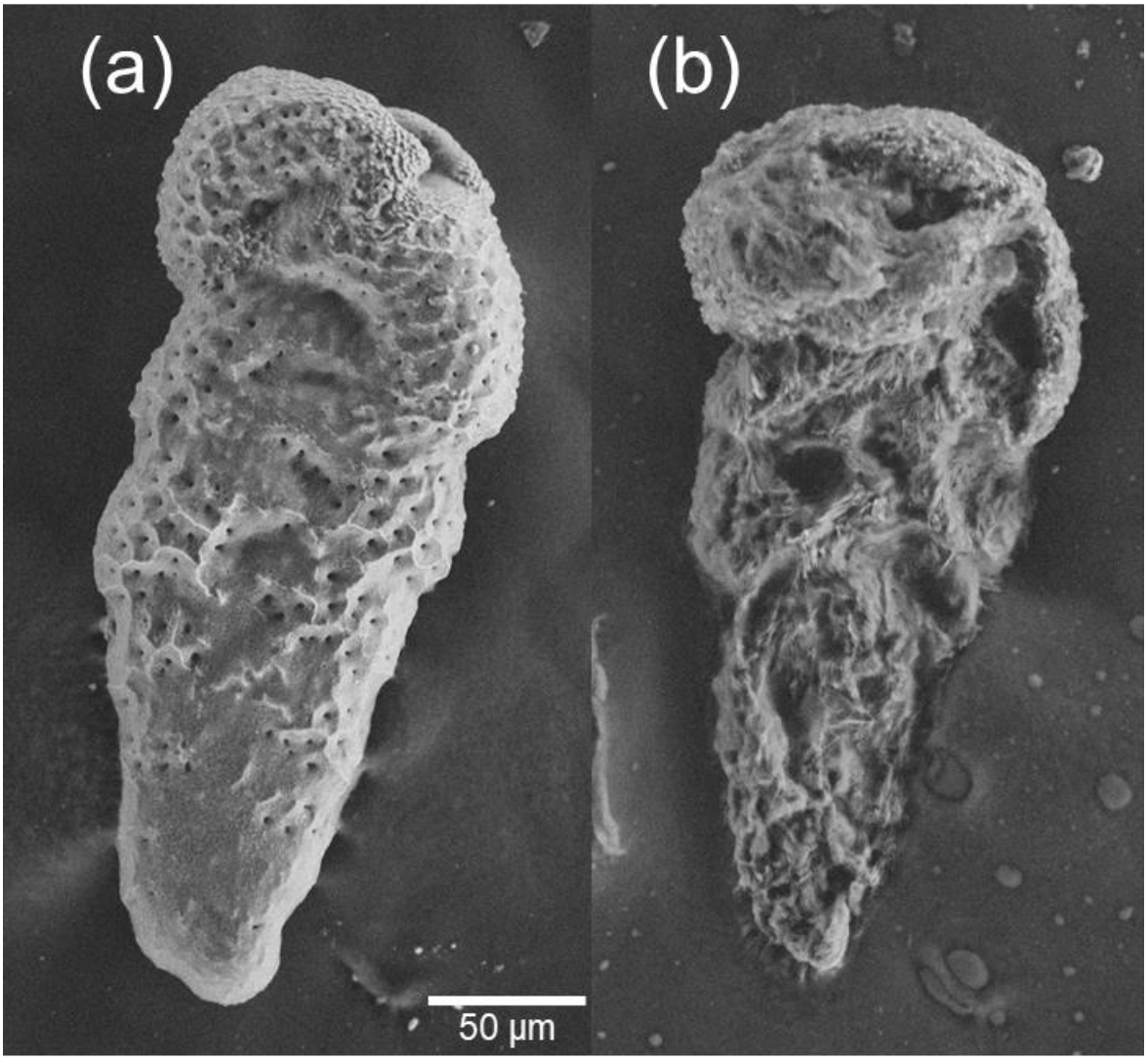

Fig. S10: SEM images of *Bolivina variabilis* before (a) and after (b) decalcification using EDTA. Specimen from a strain cultured at the Japan Agency for Marine Earth Science and Technology (JAMSTEC) in Japan .

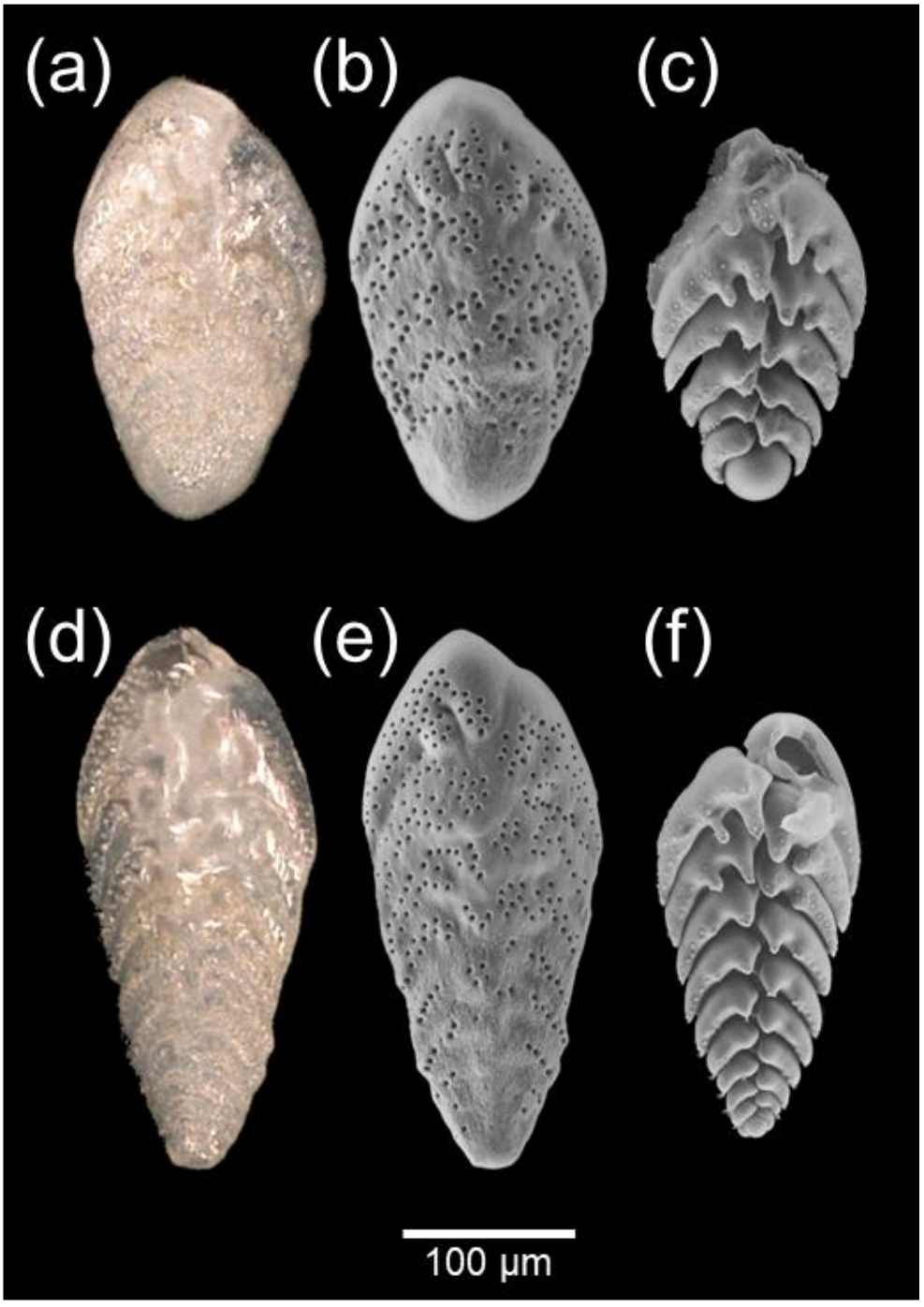

120

Fig. S11: ***Bolivina*** **sp. sampled from Off Misaki site (Sagami Bay, 740 m depth). Macrospheric (a–c) and microspheric (d–f) specimen, imaged with stereomicroscope (a and d) and low-vacuum SEM before (b and e) and after (d and f) decalcification with EDTA to expose the underlying structure below the calcitic shell. Main differences with** ***B. spissa*** **are the absence of costae on the proloculus side (before decalcification) and the presence of "horn-like" structures pointing toward the proloculus (after decalcification).**

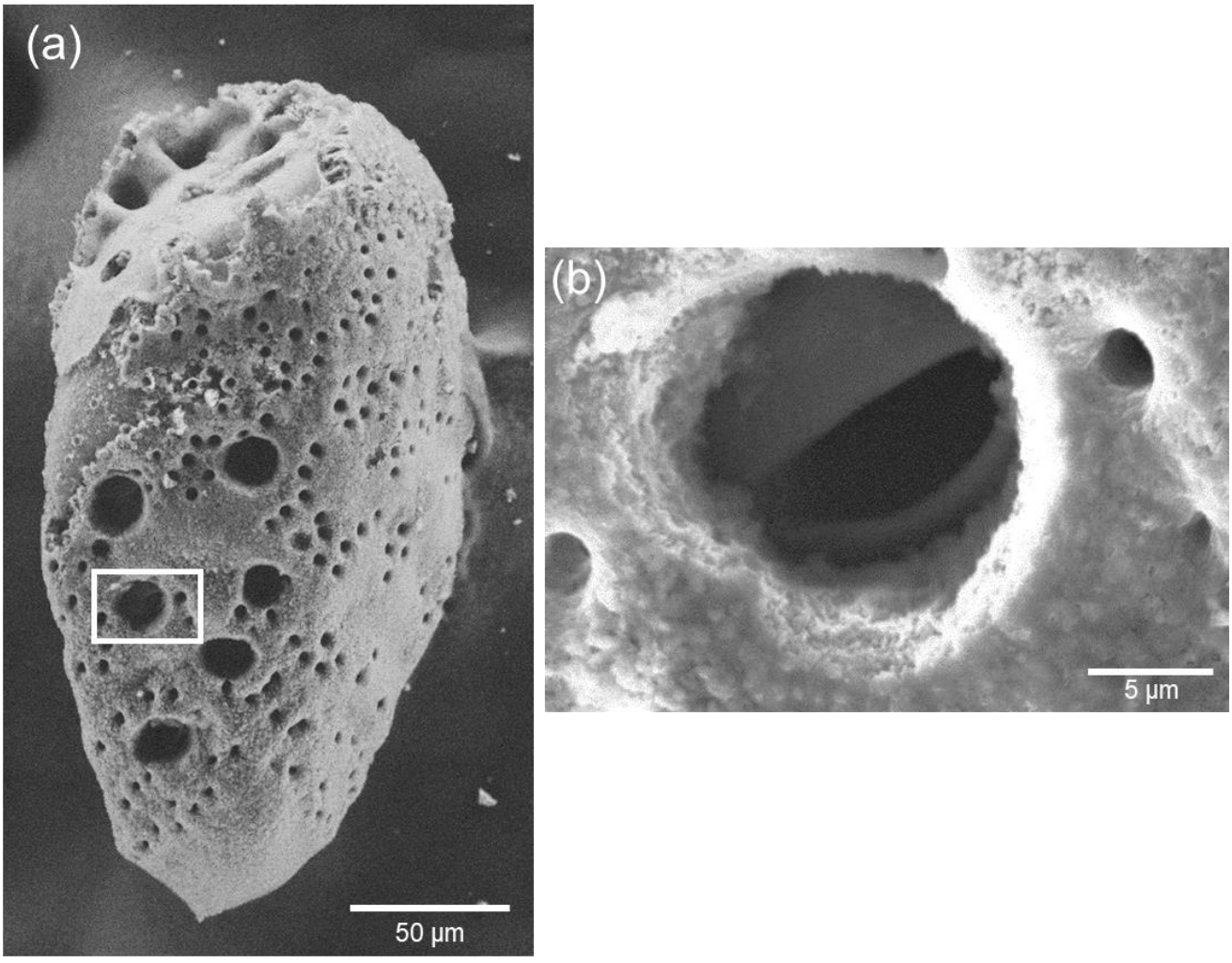

Fig. S12: (a) Drilling marks on a dead specimen of *Bolivina* sp. from Off Misaki site (Sagami Bay, 740 m depth). Note that the underlying structure is not fully bored compared to the calcitic part of the test (b).

Table S1: Si layer thickness in µm, average and standard deviation (sd) regarding chamber number, numbered from the proloculus. The total number of visible chambers (excluding proloculus) is indicated between brackets below the individual ID. N/A=not available.

Chamber	Ind. 1 (14 chambers)	Ind. 2 (14 chambers)	Ind. 3 (13 chambers)	Ind. 4 (12 chambers)	Ind. 5 (15 chambers)	Ind. 6 (13 chambers)	Ind. 7 (12 chambers)	Average	sd
Proloculus	1.60	1.10	1.65	1.45	1.45	N/A	1.20	1.41	0.22
1	1.05	0.65	0.70	0.50	0.55	0.80	0.45	0.67	0.21
2	0.60	0.45	0.50	0.40	0.45	0.40	0.35	0.45	0.08
3	0.50	N/A	0.35	0.35	0.25	0.25	0.32	0.34	0.09
4	0.45	0.30	0.25	0.27	0.25	0.15	0.30	0.28	0.09
5	0.35	N/A	0.20	N/A	0.20	0.15	0.18	0.22	0.08
6	0.30	0.30	0.15	0.25	0.20	0.15	0.15	0.21	0.07
7	0.23	N/A	0.15	N/A	0.20	0.15	0.15	0.18	0.04
8	0.20	0.25	0.15	0.15	0.15	N/A	0.10	0.17	0.05
9	0.20	N/A	0.13	N/A	0.12	N/A	0.10	0.14	0.04
10	0.15	0.18	0.10	N/A	0.15	0.10	0.08	0.13	0.04
11	0.05	N/A	0.08	N/A	0.10	0.08	N/A	0.08	0.02
12	N/A	N/A	0.05	N/A	0.10	N/A	N/A	0.08	0.04

Table S2: Weight and isotopic measurements made on *B. spissa* proloculus and apertural sides. NA=not available.

Individual ID	Microspheric or Macrospheric	Proloculus side length (µm)	total length (µm)	$CaCO_3$ weight proloculus side (ug)	Proloculus side $\delta^{13}C$ (‰)	Proloculus side $\delta^{18}O$ (‰)	$CaCO_3$ weight aperture side (ug)	Apertural side $\delta^{13}C$ (‰)	Apertural side $\delta^{18}O$ (‰)
micro03	microspheric	110	620	0.9	-0.95	2.78	NA	NA	NA
micro05	microspheric	140	620	1.1	-1.13	2.19	NA	NA	NA
micro06	microspheric	120	480	0.8	-1.16	3.02	5.5	-1.27	3.05
micro08	microspheric	100	500	0.6	-1.11	2.23	NA	NA	NA
micro10	microspheric	100	730	0.8	-0.89	2.83	13.6	-0.86	3.08
micro14	microspheric	50	240	0.2	-2.31	1.40	1.1	-1.02	3.11
macro01	macrospheric	80	560	3.8	-1.29	2.34	NA	NA	NA
macro03	macrospheric	190	640	2.3	-0.69	3.09	NA	NA	NA
macro05	macrospheric	120	570	1.5	-0.97	2.94	7.3	-1.03	2.11
macro06	macrospheric	200	570	2.9	-0.72	2.70	NA	NA	NA
macro09	macrospheric	130	330	1.2	-1.09	2.89	NA	NA	NA
macro10	macrospheric	160	650	1.7	-1.01	2.79	NA	NA	NA
macro11	macrospheric	100	290	0.8	-0.93	2.99	1.8	-1.18	2.95
macro14	macrospheric	100	290	0.8	-1.13	2.95	NA	NA	NA
macro17	macrospheric	100	310	0.8	-1.38	2.03	2.3	-1.42	2.93
macro18	macrospheric	60	260	0.5	-1.65	2.48	NA	NA	NA
macro19	macrospheric	100	220	0.9	-2.36	0.13	1.1	-0.67	2.89